



Josephson Fluxonic Diode as a Pixel with Radiation Pumping of Fluxons in Gigahertz Imaging Systems

Hamed Mehrara¹ · Farshid Raissi² · Alireza Erfanian¹

Received: 5 August 2018 / Accepted: 21 September 2018 / Published online: 10 November 2018
© Springer Science+Business Media, LLC, part of Springer Nature 2018

Abstract

Josephson fluxonic diode (JFD) has been studied and applied for gigahertz (GHz) imaging using the principle of generation of fluxons by an irradiated standing wave at gigahertz frequencies. In this device, the creation, movement, and dynamics of fluxon and anti-fluxon pairs as the magnetic field carriers in JFD have been examined in two separate modes of operation including forward and reverse bias. In both modes, the high nonlinearity feature is used for electromagnetic radiation detection. To verify this capability, an experimentally fabricated JFD based on Nb/AlO_x/Nb trilayer technology has been deployed without being coupled to any patterned antenna or frontal optics. Also, the junction design parameters and DC biasing values have accordingly been chosen to achieve the best sensitivity to gigahertz radiations. As a result, the device well respond to the specified frequency, and an image is acquired at 71 GHz which proves the potential application of JFD as a pixel of the millimeter wave imaging systems with the direct detection mechanism.

Keywords Fluxon · GHz imaging · Josephson fluxonic diode · Millimeter wave · Superconducting detector

1 Introduction

Imaging in gigahertz (GHz) and sub-terahertz (THz) wave regions of the electromagnetic spectrum (3–300 GHz) has been of great interest in the recent decades. GHz frequencies—in both active and passive imaging modes—have been widely used in the area of security screening due to their unique combined features of penetration and resolution [1–4] and in astrophysical radiometry, because of their sensitivity to emissions from astronomical objects [5–8]. Before these types of high-frequency imaging come into widespread use, the infrared imaging of blackbody radiation, which is now a highly developed technology, covered the same application area [9, 10]; however, GHz knowledge leads to a surge of research interest and outstanding

progress in developing cost-effective, high-performance, high-frequency components, and systems [11–13]. For GHz imaging purposes, compact solid-state detectors with high-sensitivity, wideband-frequency coverage, and large arrays are required. At the top of these kinds of detectors, superconducting devices, including small tunnel junction (STJ) [14–16], long Josephson junction (LJJ) [17–19], single-photon detector (SPD) [20, 21], transmission edge sensor (TES) [22–24], kinetic inductance detector (KID) [25–27], and superconducting bolometers [28–31] are excellent options due to their distinctive advantages of extremely low noise and high-frequency operation. They have proven to be the most sensitive GHz detector duo to the quantum limits of noise in low/ultra-low-temperature superconducting devices (LTS/ULTS) [32–34]. More importantly, they are fabricated by the current micro- or nanolithography techniques and consequently can be built into large arrays [35–38].

Compared with the existing LTS detectors, Josephson fluxonic diode—which works at 4 K—provides distinct advantages including, having an inherent gain, determining the frequency, and amplitude of radiation simultaneously, as well as having a simple addressing scheme. Its size can be adjusted to provide an antenna-less detector [39, 40]. In principle, JFD is a long Josephson junction that is filled with spatially reversing magnetic fields. Half of this junction contains vortices (also called fluxons or solitons)

Electronic supplementary material The online version of this article (<https://doi.org/10.1007/s10948-018-4897-z>) contains supplementary material, which is available to authorized users.

✉ Alireza Erfanian
erfanian@mut.ac.ir

¹ Department of Electrical Engineering, Malek-Ashtar University of Technology, Tehran, Iran

² Department of Electrical Engineering, K.N. Toosi University of Technology, Tehran, Iran

and the other half is filled with anti-vortices [41]. Figure 1 demonstrates the configuration used for a JFD with a T-shaped control line (which can be isolated from the Josephson junction).

The control line creates a magnetic field which reverses its direction at the center of the long Josephson junction. It has a rectifying type of DC current–voltage curve—similar to a semiconductor PN junction—used to detect incoming radiation in the millimeter and sub-millimeter frequencies [39]. The detection mechanism in JFD is based on the creation of vortex–antivortex pairs due to radiation coupling to its length in the reverse bias mode. Theoretically, the upper detection frequency of a JFD is limited to around 700 GHz for Nb technology (the gap voltage of niobium ~ 2.8 meV), but in practice, it would be fewer due to the geometrical limitation and the length that may be used to fabricate the detector.

In this study, for the first time, we focus on developing a GHz imager using one single-pixel JFD without any antenna couple to this device. We also propose the concept of millimeter wave (MMW) imaging with standing waves. For this goal, in the beginning, the use of this device as MMW detector is theorized and formulated. Then, in the experimental section, after describing the fabrication parameters, the suitable DC bias value of JFD is chosen to conclude the best sensitivity at the imager. After that, the frequency of imaging will be tuned from the responsivity spectrum and finally, a GHz image is captured as a proof of the concept.

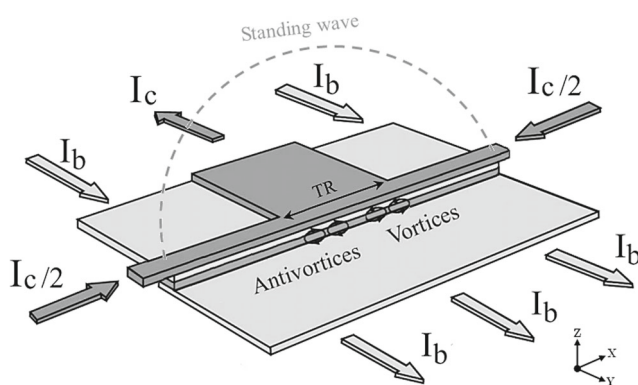


Fig. 1 The configuration of Josephson Fluxonic Diode (JFD): the control current (I_C) is applied into two wings of control line (dark gray solid on top) equally and obtained from the transition region (TR). It creates a spatially reversing magnetic field and produces vortices and anti-vortices in each wing of the Josephson junction. The bias current (I_b) is uniformly applied to the top electrode of the long Josephson junction with the length of L and goes out from the base electrode (light gray solids). This causes the vortices and anti-vortices in the junction to be moved by a Lorentz force. Also, the incoming RF radiation creates a standing wave (gray dashed line with the peak at the center) which induces an oscillating current in corresponding Josephson cells

2 Theory of Operation

As illustrated in Fig. 1, a control current is fed to two wings of the control line of JFD and taken from it in the middle. This induces the opposite magnetic fields in these two separated regions inside the underneath long Josephson junction. Vortices fill one half and anti-vortices fill the other half of the junction. As can be seen from this figure, the region where the direction of magnetic field changes is called the transition region (TR), and its size is about the width of the T-shaped control line at the center. Vortices and anti-vortices attract each other and in the equilibrium state, JFD cannot have a steady-state movement of vortices or anti-vortices; therefore, a so-called the built-in current is set up in the transition region that pushes them away from each other and compensates the attraction force (like built-in potential in PN junction). The change in the magnetic field in the transition region can be used to obtain the magnitude of the built-in current both by Ampere's law and the Josephson relations [42].

By applying a uniform bias current to the junction, the pairs are either pushed toward each other or are pushed away toward their points of entry at the boundaries. The direction of the bias current determines whether they are forced to or away from each other. When the bias current is in the opposite direction to the built-in current, the attraction force between vortices and anti-vortices take over, and they move toward each other. Once the bias current is in the same direction as the built-in current, they have pushed away from each other. Similar to a PN junction diode, these two directions of bias current are named the forward and reverse bias. This naming is appropriate because the forward and reverse bias IV curves are drastically different and asymmetric with a near-linear characteristic in forward bias and a short circuit in reverse bias mode.

Also, there is a so-called breakdown (or maximum zero-voltage) current in JFD in which the junction falls into a voltage state by a sudden creation of fluxons and anti-fluxons at the middle of the junction in deep reverse bias. When JFD is reverse biased at this point, an incoming radiation can boost the pair generation anywhere along the junction and lead to a voltage. Earlier, the best sensitivity to microwave signals has been explained and evaluated at breakdown [39]. At this state, the fluxon pairs are created in the middle of TR by small amplitude radiation that comes from increasing the current box value and flow in the junction using the applied bias current due to the Lorentz force. This is analogous to the PN diode in which electron-hole pairs are created in the depletion region due to the absorbing of radiation in the reverse bias and jump the output current.

If the total length of JFD along x -axis (L) is proportional to the wavelength of the incoming radiation, due to

interference between waves reflected back and forth at the device’s boundaries, then a standing wave is generated along the JFD. This standing wave can interact with the moving fluxons or create them in some specific conditions which will be addressed later in this article. The location of oscillation peak in this standing wave is fixed. Though the oscillations with the peak at the center of JFD can change the Josephson phase and lead to the breakdown of JFD in the reverse bias. Hence, in this mode, the device can ideally respond to the wavelength equal or lower than twice the length of JFD. By choosing the bias current near the breakdown current and waiting for the generation of the vortex-antivortex pairs in the middle of TR, one can conclude that topmost amplitude of the GHz wave oscillations should be at the center of JFD to help pair generation. The corresponding radiation resembles a half sine standing wave (as depicted in Fig. 1 with a gray dash line), which breaks the junction and pumps the fluxons.

To gain some insight into the dynamics of the JFD, we make use of the resistively and capacitively shunted junction (RCSJ) model [43]. This model describes the sine-Gordon equation of a long Josephson junction and also JFD, as well, because they both consist of some distributed lumped Josephson junctions consecutively. Figure 2 represents this model [41]. In this model, each JFD’s element, which is highlighted by dashed boxes, consists of three parts including the Josephson junction box, transmission line box, and the input currents box as shown from the bottom to the top. The lumped Josephson element is represented by a nonlinear differential inductor L_J , shunted by a capacitor C and a resistor R_{sg} per unit length of the junction. The capacitor element shows the displacement current due to the geometric shunting capacitance, and the resistive element defines the subgap resistance below the gap voltage of the superconducting junction. Differential equation related

to applied bias current density versus the voltage in this element of RCSJ model is:

$$J(x) = J_c \sin(\phi) + \frac{V}{R_{sg}} + C \frac{dV}{dt}, \tag{1}$$

where J_c is the critical current density of the Josephson junction element.

To model the effect of the transmission lines between neighboring Josephson elements in the experimental device, the parallel array of Josephson junctions must be coupled via a shunted inductor-resistor elements [41]. In this box, the geometric inductance per unit length of the superconducting electrode of JFD is shown by L_s , while R_c indicates the surface resistance of this electrode of the Josephson junction in the unit length. The dynamic equation describing the behavior of each unit cell of JFD will be completed with the application of the bias, control, and RF currents as derived in [44]:

$$\begin{aligned} \alpha \phi_{xxt} + \phi_{tt} - \phi_{xx} + \frac{1}{\sqrt{\beta}} \phi_t + \sin \phi &= \rho_{in} \\ \rho_{in} &= \rho_b(x) + \rho_c(x) + \rho_\omega \sin \Omega t \end{aligned} \tag{2}$$

In (2), $\varphi(x, t)$ indicates the phase difference of each distributed element of JFD in which the corresponding voltage can be calculated by time derivate of the phase difference (φ_t). Other parameters are as follows: α is defined by $\omega_J L_s / R_c$; ω_J is the Josephson plasma frequency given by $[2\pi J_c R_{sg}^2 C / \Phi_0]^{1/2}$; Φ_0 is the flux quantum unit; β is the Stewart–McCumber parameter which equals to $2\pi R_{sg}^2 C / \Phi_0$; Ω is the angular frequency of incoming RF radiation; ρ_ω is the maximum of induced current by this radiation; ρ_c is the applied DC control current; and ρ_b is the bias current. For simplicity, all spatial parameters are scaled in units of the Josephson penetration depth

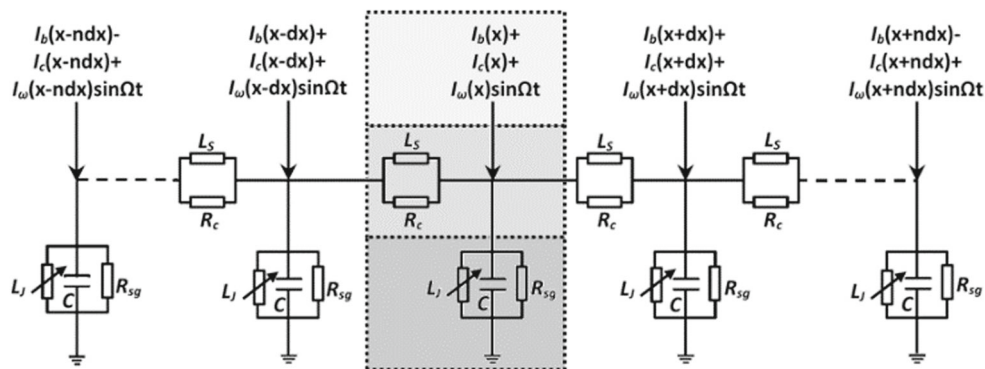


Fig. 2 This model is used for simulation of the JFD. It includes ideal Josephson junctions in a series represented by a nonlinear inductor in parallel with a capacitor C and a resistor R_{sg} . They are connected through a parallel combination of an inductor and a resistor. Each element (in dashed boxes) is extended around origin “ x ” in two directions

for n times. The current solution of this model gives us fluxons that are current vortices, travel along the junction. Here, I_b , I_c , and I_ω are, respectively, the value of applied bias current, control current, and amplitude of induced RF current in each cell

(λ_J), the temporal parameters are scaled in units of the inverse Josephson plasma frequency; and current amplitude is scaled by J_c .

The solution of (2) can be reached by simulating the equivalent circuit presented in Fig. 2 via the finite difference method. The applied currents cause the left hand of (2) to be changed. For simulation purposes, we should determine the bias, control, and microwave spatial current distribution in Fig. 1. Based on this configuration which is experimentally verified [42], the bias current is distributed homogeneously along the length of JFD. The control current is simulated by feeding a current directly to the end elements; then this current is collected from the cells in the transition region where the built-in current is created. Moreover, based on the assumption that the length of JFD is about one half wavelength of microwave irradiation, a sine-standing wave, $\sin(\pi x/L)$, is induced along the junction in the x -direction. In practice, it is possible to achieve the T-shaped control line of JFD which acts as a half-wave antenna.

Based on the abovementioned current distribution, the feeding current for the first and last elements of JFD is:

$$\rho_{in}|_{x=\pm L/2} = \rho_b(x) - \rho_c(x), \tag{3}$$

where $\rho_c(L/2) = I_c/2$ and $I_c = \int \rho_c(x)dx$. The condition of the corresponding elements in the transition region is affected by serving bias and control current plus the rf-induced current contributions:

$$\rho_{in}|_{x=TR} = \rho_b(x) + \rho_c(x) + \rho_\omega \sin\left(\frac{\pi x}{L}\right) \sin \Omega t, \tag{4}$$

And the other elements only include the bias current impact and RF contributions, so

$$\rho_{in}|_{x \neq \pm L/2, x \neq TR} = \rho_b(x) + \rho_\omega \sin\left(\frac{\pi x}{L}\right) \sin \Omega t, \tag{5}$$

In order to investigate how the standing wave creates fluxons, 1000 unit cells (including 300 elements for TR), with the condition specified in (2)–(5) are simulated in MATLAB.

For each node along the x -axis, the solution of the voltage and consequently φ (see (2)) are obtained at the steady state in which $d\varphi/dx$ suggests the magnetic vortices travel along the length of JFD. The time-evolution results of creation and pumping of vortices as well as anti-vortices under the application of a GHz excitation, are presented in Fig. 3.

The conditions at which this simulation is carried out are as follows: $L = 1000 \mu\text{m}$ (each cell has $1 \mu\text{m}$ length), $\beta = 10$, time step = 0.05 pSec, total simulation time = 500 pSec, $R_{sg} = 0.86 \Omega/\mu\text{m}$, $R_c = 0.44 \Omega/\mu\text{m}$, $L_s = 0.0025 \text{pH}/\mu\text{m}$, and $C = 0.0035 \text{pF}/\mu\text{m}$, the angular frequency of RF irradiation is equal to $0.1 \omega_J$, $\rho_c = 0.15$, and JFD is biased closed to the breakdown in the reverse bias with $\rho_\omega = 0.01$. Full animation of this evolution is provided in Online Resource 1.

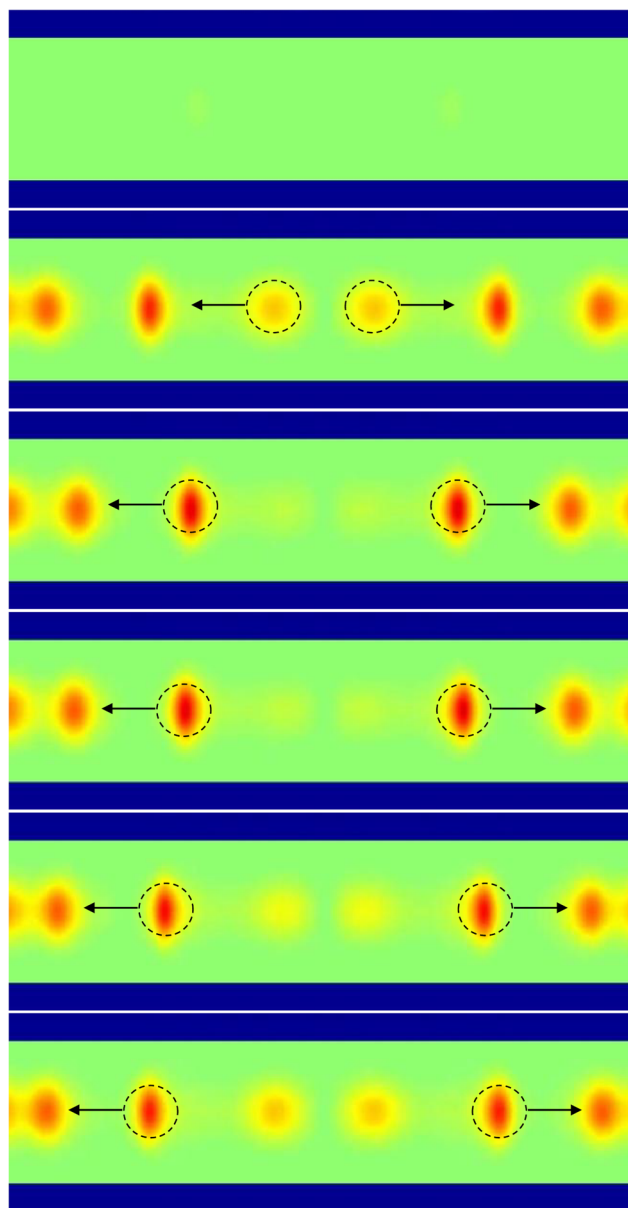


Fig. 3 The time evolution of creation and pumping of vortices and anti-vortices along the length of JFD is extracted using $d\varphi/dx$. The device is biased closed to the breakdown point in the reverse bias under application of half-wave gigahertz excitation with the amplitude of $\rho_\omega = 0.01$ (as depicted in Fig. 1). Other parameters are as follows: $L = 1000 \mu\text{m}$, $\beta = 10$, the angular frequency of RF irradiation is equal to $0.1 \omega_J$ and $\rho_c = 0.15$. The first picture depicts the condition in which no fluxons can be generated. Continuously, one vortex-antivortex pair is created by gigahertz excitation in the middle of the junction and pushed away to the boundaries (shown by a dashed circle around them which indicate their movement direction)

3 Experimental Test

Fabricated JFD is based on Nb/AIO_x/Nb trilayer process on a Si wafer with a thickness of 500 nm SiO₂. This

layer has been grown by the wet oxidation process. The Nb and Al layers are DC-magnetron sputtered in the argon atmosphere. Also, the dry oxidation of the Al is performed in pure oxygen. The thicknesses for the base electrode, Al layer, and the top electrode are about 200, 6, and 100 nm, respectively. Also, JFD’s outline is patterned using the standard photolithography techniques to form the final devices. So, the patterned length of the junction measured about 1000 μm with 40 μm width and the transition region of 300 μm . The electrical test of the fabricated device with the emphasis on DC biasing with spectrum response analysis and setup the GHz imager is done after.

In practice, when the sum of the built-in current and the reverse bias current exceeds the local critical current of the single junction at any space, vortices and anti-vortices pair can generate from the corresponding cell. It is because the local $\varphi(x)$ of the junction slips by 2π . The consequent generation and movement of these pairs cause a sudden change in the output voltage. In reality, the incoming radiation can be coupled to the JFD’s control or bias line or both of them [40]. To reach the best sensitivity, the JFD is

DC biased near the breakdown to detect incoming radiation properly. The measured DC IV curve for fabricated JFD at 4 K in its reverse bias mode with control current of 4 mA is provided in Fig. 4a. As can be seen, the maximum zero-voltage current which is the breakdown point, is equal to 15 mA. It is less than the critical current of the device, 30 mA that was measured by a small Josephson junction, fabricated near the JFD. It is observed that it decreases with increasing control current which is in agreement with theory [45].

Further increasing the bias current causes the junction to go into a flux flow branch whose voltage is a function of the control current, and in this mode, the pair’s generation continuously goes on (see Online Resource 1). For testing the GHz imaging, the device is biased, less than 15 mA with the selected control current (point A in Fig. 4a). Practically, as the radiation is pumped to the JFD, the junction jumps into a voltage state (point B in Fig. 4a). Remarkably, by removing the radiation, it turns back to its zero-voltage step.

To analyze the spectral responsivity of fabricated JFD, a source of GHz radiation was used to pump frequencies from 55 to 110 GHz and record the voltage changes. The consistent responsivity is also analytically simulated to compare with the measurement. They are both presented in Fig. 4b. As it can be seen, the accepted simulation power has two peaks at 76.5 and 102 GHz (red circles) which is about -7.2 and -5 dB, respectively, and in the other frequencies, the majority of the power reflected. Measuring the detected voltage drop on the JFD’s bias terminals follows the same behavior, but the peak frequencies have been shifted to lower frequencies (blue squares). This is probably because the simulated structure does not contain all wiring routes from the device to the output readout pads and the effective length is different from its actual length.

The Josephson fluxonic diode detector was successfully prepared for the imaging mode. From the last results presented in Fig. 4b, the optimal frequency of imaging is chosen to be 71 GHz. The system setup is shown in

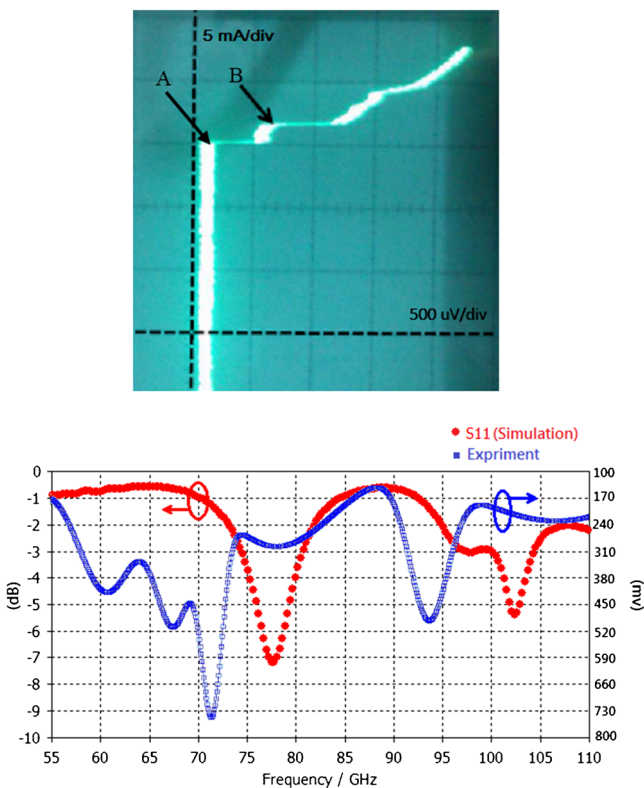


Fig. 4 a Experimental DC IV curves of the reverse bias JFD with 4 mA control current. For the gigahertz imaging, the device is biased at the point “A” and the radiation causes a jump into the voltage in point “B.” The length of the fabricated JFD is about 1000 μm with 40 μm width and the transition region of 300 μm . b The simulated delivered power to control line (red circles) and measured readout voltage drop across JFD’s electrodes by pumping RF radiation

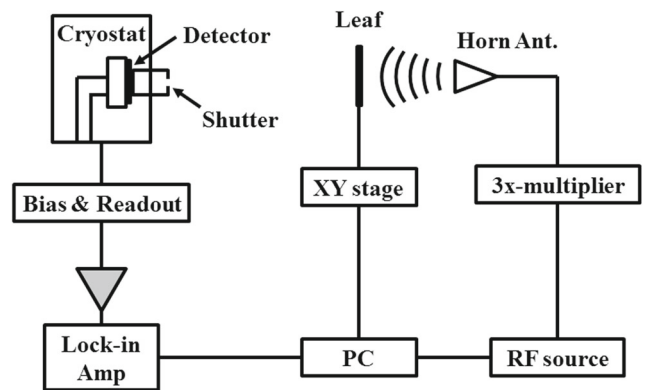


Fig. 5 Schematic of the gigahertz imaging setup

Fig. 5. A GHz source of 10–40 GHz with one $3\times$ multiplier and a W-band horn antenna is used to generate tunable CW radiation. The fabricated JFD and wiring pads were mounted on the cold head of cryostat and irradiated with the aforementioned RF source through a metallic adjustable shutter window out of the cryostat. Each time a signal was detected, the shutter is closed to capture the reference

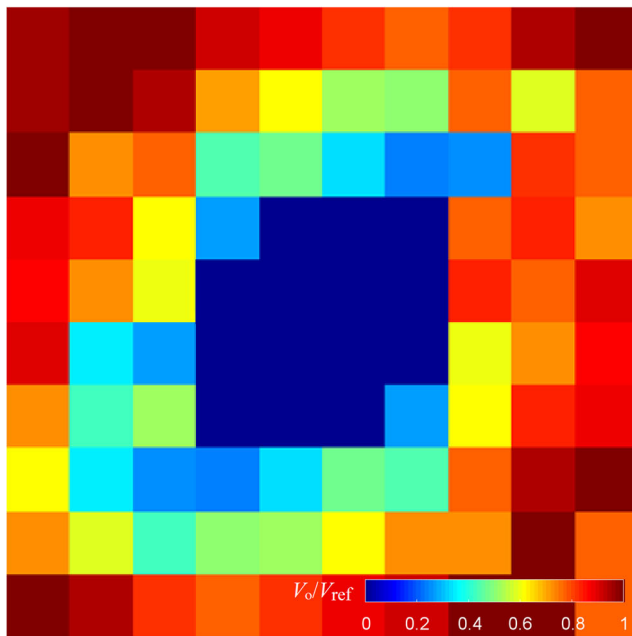


Fig. 6 The captured image of a fresh Solenostemon leaf with a single JFD at 71 GHz. The optical photo of the sample which was mounted on a piece of paper and cover with a plastic shelf is also depicted

signal. No optical system or focusing mirrors was used to concentrate the beam on the detector. For imaging, a fresh Solenostemon leaf sample was used to face in front of the detector. By raster scanning the sample using a linear XY stage positioner, the transmission property of the sample was taken at 71 GHz. The spot size of the imaging system was limited to approximately 3 mm using the shutter and the typical scan resolution was 5 mm. The junction biased just below maximum zero-voltage and the absolute voltage changes induced by the incident radiation acquired and amplified by a preamplifier operated at room temperature. This was done by a lock-in amplifier synchronized with a 1-kHz bias current to minimize the noise. This amplifier also averaged the signal for 3 s, and then the output DC signal was recorded and processed by a computer to reconstruct the final image.

Figure 6 displays the result of the captured image by a single JFD detector at 71 GHz from the sample. Figure 6a shows the visible image of the Solenostemon leaf mounted on a piece of paper and covered with the plastic shelf, and Fig. 6b shows the equivalent 71 GHz transmission image. The depicted image has been adjusted (with normalizing the output voltage to the reference voltage, i.e., V_o/V_{ref}) to show the minimum and maximum signal as the blue and red colors, respectively. This image was acquired in a frame of 10×10 pixels. The integration time was 3 s/pixel, and the reference signal was picked up at 1 s/pixel. Despite the low resolution of this image, it highlights the key feature of GHz imaging whereby the millimeter wave radiation is absorbed by the water in the leaf and gives a contrast to see the sample. However, we believe that an array of such a device can significantly reduce the scanning time and further improve the resolution for GHz imaging systems.

4 Conclusion

We have successfully theorized, fabricated, and demonstrated the GHz imaging using a single Josephson fluxonic diode on the basis of standing wave pumping of the fluxons pair. Biasing the JFD near the maximum zero-voltage current in the reverse bias potentiate the phase of the Josephson junction in the transition region to be 2π -slipped by a standing wave proportional to the length of JFD. In millimeter length of this device, the range of detectable frequencies falls into the GHz band. This device with no additional antenna was constructed to test the ability of capturing an image at 71 GHz. The final image approved the sensitivity of JFD to GHz standing wave radiation by absorbing the water and making a contrast to see the sample. This work has demonstrated the potential usage of the JFD as a sensitive GHz detector for LTS imaging array.

Acknowledgements The authors wish to thank Dr. Mahdi Khajeh for his important contribution to the experimental effort and technical support.

References

- Gao, X., Li, C., Gu, S., Fang, G.: Study of a new millimeter-wave imaging scheme suitable for fast personal screening. *IEEE Antennas Wirel. Propag. Lett.* **11**, 787–790 (2012)
- Gumbmann, F., Schmidt, L.: Millimeter-wave imaging with optimized sparse periodic array for short-range applications. *IEEE Trans. Geosci. Remote Sens.* **49**(10), 3629–3638 (2011)
- Appleby, R., Anderton, R.N.: Millimeter-wave and submillimeter-wave imaging for security and surveillance. *Proc. IEEE* **95**(8), 1683–1690 (2007)
- Sinclair, G.N., Appleby, R., Coward, P.R., Price, S.: Passive millimeter-wave imaging in security scanning. In: *Passive Millimeter-Wave Imaging Technology IV*, pp. 40–46. International Society for Optics and Photonics (2000)
- Robertson, D.A., Macfarlane, D.G.: A 94 GHz dual-mode imaging radarometer for remote sensing. In: *Passive Millimeter-Wave Imaging Technology IX*, p. 621102. International Society for Optics and Photonics (2006)
- Sasaki, A.-I., Nagatsuma, T.: Millimeter-wave imaging using an electrooptic detector as a harmonic mixer. *IEEE J. Selected Topics Quant. Electron.* **6**(4), 735–740 (2000)
- Du, J., Hellicar, A., Li, L., Hanham, S., Nikolic, N., Macfarlane, J., Leslie, K.: Terahertz imaging using a high-Tc superconducting Josephson junction detector. *Supercond. Sci. Technol.* **21**(12), 125025 (2008)
- Kleine-Ostmann, T., Schrader, T., Bieler, M., Siegner, U., Monte, C., Gutschwager, B., Hollandt, J., Steiger, A., Werner, L., Müller, R.: THz metrology. *Frequency* **62**(5–6), 137–148 (2008)
- Vollmer, M., Klaus-Peter, M.: *Infrared Thermal Imaging: Fundamentals, Research and Applications*. Wiley (2017)
- Rogalski, A.: *Infrared Detectors*. CRC Press (2010)
- Popovic, Z., Grossman, E.N.: THz metrology and instrumentation. *IEEE Trans. Terahertz Sci. Technol.* **1**(1), 133–144 (2011)
- Amirmazlaghani, M., Raissi, F.: Feasibility of roomtemperature GHz-THz direct detection in graphene through hotcarrier effect. *IEEE Transactions on Device and Materials Reliability* (2018)
- Amirmazlaghani, M., Raissi, F.: Graphene-based detector for w-band and terahertz radiations. Google Patents (2018)
- Ariyoshi, S., Otani, C., Dobroiu, A., Sato, H., Kawase, K., Shimizu, H., Taino, T., Matsuo, H.: Terahertz imaging with a direct detector based on superconducting tunnel junctions. *Appl. Phys. Lett.* **88**(20), 203503 (2006)
- Tucker, J.R., Feldman, M.J.: Quantum detection at millimeter wavelengths. *Rev. Mod. Phys.* **57**(3), 1055 (1985)
- Day, P.K., LeDuc, H.G., Mazin, B.A., Vayonakis, A., Zmuidzinas, J.: A broadband superconducting detector suitable for use in large arrays. *Nature* **425**(6960), 817 (2003)
- Chevriaux, D., Khomeriki, R., Leon, J.: Theory of a Josephson junction parallel array detector sensitive to very weak signals. *Phys. Rev. B* **73**(21), 214516 (2006)
- Nagatsuma, T., Enpuku, K., Irie, F., Yoshida, K.: Flux-flow type Josephson oscillator for millimeter and submillimeter wave region. *J. Appl. Phys.* **54**(6), 3302–3309 (1983)
- Zhang, Y., Winkler, D., Claeson, T.: Detection of mm and submm wave radiation from soliton and flux-flow modes in a long Josephson junction. *IEEE Trans. Appl. Supercond.* **3**(1), 2520–2523 (1993)
- Hadfield, R.H.: Single-photon detectors for optical quantum information applications. *Nat. Photonics* **3**(12), 696 (2009)
- Eisaman, M.D., Fan, J., Migdall, A., Polyakov, S.V.: Invited review article: Single-photon sources and detectors. *Rev. Sci. Instrum.* **82**(7), 071101 (2011)
- Kuo, C., Bock, J., Bonetti, J., Brevik, J., Chattopadhyay, G., Day, P., Golwala, S., Kenyon, M., Lange, A., LeDuc, H.: Antenna-coupled TES bolometer arrays for CMB polarimetry. In: *Millimeter and Submillimeter Detectors and Instrumentation for Astronomy IV*, p. 70201I. International Society for Optics and Photonics (2008)
- Westbrook, B., Lee, A., Meng, X., Suzuki, A., Arnold, K., Shirokoff, E., George, E., Aubin, F., Dobbs, M., MacDermid, K.: Design evolution of the spiderweb TES bolometer for cosmology applications. *J. Low Temp. Phys.* **167**(5–6), 885–891 (2012)
- Duncan, W.D., Holland, W.S., Withington, S., Zmuidzinas, J.: Millimeter and submillimeter detectors and instrumentation for astronomy IV. In: *Proc. SPIE* (2008)
- Schlaerth, J., Vayonakis, A., Day, P., Glenn, J., Gao, J., Golwala, S., Kumar, S., LeDuc, H., Mazin, B., Vaillancourt, J.: A millimeter and submillimeter kinetic inductance detector camera. *J. Low Temp. Phys.* **151**(3–4), 684–689 (2008)
- Monfardini, A., Swenson, L., Bideaud, A., Désert, F., Yates, S., Benoit, A., Baryshev, A., Baselmans, J., Doyle, S., Klein, B.: NIKA: A millimeter-wave kinetic inductance camera. *Astron. Astrophys.* **521**, A29 (2010)
- Baselmans, J.: Kinetic inductance detectors. *J. Low Temp. Phys.* **167**(3–4), 292–304 (2012)
- Seidel, P.: *Applied Superconductivity: Handbook on Devices and Applications*. Wiley (2015)
- Cherednichenko, S., Drakinskiy, V., Berg, T., Khosropanah, P., Kollberg, E.: Hot-electron bolometer terahertz mixers for the Herschel space observatory. *Rev. Sci. Instrum.* **79**(2), 034501 (2008)
- Kuzmin, L.S., Chiginev, A.V.: Multichroic bandpass seashell antenna with cold-electron bolometers for CMB measurements. In: *Millimeter, Submillimeter, and Farinfrared Detectors and Instrumentation for Astronomy VIII*, p. 99141U. International Society for Optics and Photonics (2016)
- Richards, P.: Bolometers for infrared and millimeter waves. *J. Appl. Phys.* **76**(1), 1–24 (1994)
- Grossman, E.N., Dietlein, C., Bjarnason, J.E., Ramirez, M., Leivo, M., Penttila, J., Helisto, P., Luukanen, A.: Imaging with modular linear arrays of cryogenic Nb microbolometers. In: *Passive Millimeter-Wave Imaging Technology XI*, p. 694806. International Society for Optics and Photonics (2008)
- Humphreys, R., Hirst, P., Heath, R., Elliner, D., Parker, N., Smith, M.A.: Passive mm-wave imager using HTS Josephson junction detectors. In: *Passive Millimetre-Wave and Terahertz Imaging and Technology*, pp. 59–70. International Society for Optics and Photonics (2004)
- Noroozian, O.: Superconducting microwave resonator arrays for submillimeter/far-infrared imaging. California Institute of Technology (2012)
- Tang, Q., Barry, P., Thakur, R.B., Kofman, A., Nadolski, A., Vieira, J., Shirokoff, E.: Fabrication of antenna-coupled KID array for cosmic microwave background detection. *J. Low Temp. Phys.*, 1–8 (2018)
- Allman, M.S., Verma, V.B., Stevens, M., Gerrits, T., Horansky, R.D., Lita, A.E., Marsili, F., Beyer, A., Shaw, M., Kumor, D.: A near-infrared 64-pixel superconducting nanowire single photon detector array with integrated multiplexed readout. *Appl. Phys. Lett.* **106**(19), 192601 (2015)
- Posada, C., Ade, P., Ahmed, Z., Arnold, K., Austermann, J., Bender, A., Bleem, L., Benson, B., Byrum, K., Carlstrom, J.: Fabrication of large dual-polarized multichroic TES bolometer arrays for CMB measurements with the SPT-3G camera. *Supercond. Sci. Technol.* **28**(9), 094002 (2015)

38. Mahashabde, S., Sobolev, A., Bengtsson, A., Andrén, D., Tarasov, M.A., Salatino, M., de Bernardis, P., Masi, S., Kuzmin, L.S.: A frequency selective surface based focal plane receiver for the OLIMPO balloon-borne telescope. *IEEE Trans. Terahertz Sci. Technol.* **5**(1), 145–152 (2015)
39. Raissi, F.: Simulation results on submillimeter wave detection by Josephson fluxonic diode and a method to address its focal plane array. *IEEE Trans. Appl. Supercond.* **16**(1), 38–42 (2006)
40. Vafadarali, H., Raissi, F., Erfanian, A.: Nonlinear response of Josephson fluxonic diode to radiation based on geometry and incident radiation point. *Chin. J. Phys.* **56**(1), 125–130 (2018)
41. Raissi, F.: Modeling of the Josephson fluxonic diode. *IEEE Trans. Appl. Supercond.* **13**(2), 3817–3820 (2003)
42. Raissi, F., Nordman, J.: Josephson fluxonic diode. *Appl. Phys. Lett.* **65**(14), 1838–1840 (1994)
43. Gross, R., Marx, A., Deppe, F.: *Applied superconductivity: Josephson effect and superconducting electronics*. De Gruyter (2015)
44. Mehrara, H., Raissi, F., Erfanian, A., Armaki, S.H.M., Abdollahi, S.: Dynamic microwave impedance of dc-biased Josephson Fluxonic Diode in the presence of magnetic field and rf drive. *IEEE Trans. Appl. Supercond.* **28**(4), 1–8 (2018)
45. Abdollahi, S., Raissi, F.: Numerical investigation of soliton dynamics, injection into the transition region of a soliton diode. *Physica C: Supercond.* **489**, 13–18 (2013)